Research Article **Open Access**

Myles Rooney, Francesco Carulli, Silvia Luzzati, Roland Resel, Benedikt Schrode, Riccardo Ruffo, Mauro Sassi, and Luca Beverina*

Diketopyrrolopyrrole latent pigment-based bilayer solar cells

DOI: https://doi.org/10.1515/oph-2018-0002
Received November 16, 2018; accepted December 21, 2018

Abstract: Two Diketopyrrolopyrrole based latent pigment donor materials were fabricated into thin film bilayer photovoltaic devices featuring PCBM as the acceptor. Thermal deprotection of the thin film, carried out at 200° C, returns the dye-like small molecule to the corresponding pristine pigment quantitatively. The connected evolution of electrical and morphological features of pure thin films and blends are examined. A significant decrease in extinction coefficient was noted and correlated both to intrinsic changes of the electronic structure upon cleavage and to an increase in internal scattering due to extensive crystallization. Power conversion efficiencies of 0.33% were achieved for bilayer devices, nearly doubling previous results with latent pigment DPP devices, under comparable experimental conditions.

1 Introduction

In the field of organic optoelectronics, solution processed devices are usually made by a standard bottom up build, with sequential layering of active materials. To achieve highly resolved and reproducible interlayers orthogonal solvent processing is used: the bottom layers of material are ideally completely insoluble in the solvent used to process the subsequent layers. Unfortunately, the nature of the materials commonly used in Organic Photovoltaics (OPV) are such that the solubility characteristics of two layers (donor and acceptor) are often very similar. Completely orthogonal solvent approaches are thus quite rare. Generally, what occurs is a fine intermixing of the interface between donor and acceptor. Even when completely orthogonal systems can be established, underlying layers are susceptible to swelling with the orthogonal solvent allowing for sequentially deposited materials to permeate into the bulk of the underlying layer [1]. This diffusion of organic materials is advanced by common processes such as thermal annealing. Although this intermixing at the interface can often be useful for exciton splitting in photovoltaics, the resulting reproducibility and stability remain a concern [2]. So far the only reliable way to produce stacked devices with sharp interfaces is vacuum deposition. This technology also holds the record for highest efficiency in organic, molecular based single junction solar cells [3].

The latent pigment approach may offer advantages in this respect. Latent pigments are organic pigments bearing a chemically or thermally removable functionality, which induces a non-permanent, dye-like solubility character [4]. The labile group silences inter- and intramolecular hydrogen bond networks (Figure 1). They have already demonstrated use in numerous fields such as OPV [5, 6], thermochromic devices for food industries [7], luminescent solar concentrators [8] and more recently Organic Thin Film transistors [9]. The nature of the material crystallisation through this deprotection process has been examined [4]. and the possibility of creating thin heterojunction and BHJ films from materials has been exemplified through pigments such as indigo [10, 11].

Di-tert-butyl dicarbonate (t-BOC) is the most common latent pigment protection group. It allows for facile functionalisation of pigments at near quantitative yields [12]. This functionality is sterically bulky and is successful in disrupting π-π stacking networks and H-bonding sites to afford soluble semiconductor materials. The quantitative deprotection by a thermal treatment happens in a temperature range far below the degradation point of common pigments such as diketopyrrolopyrrole (DPP), quinacridone (QC), perylenediimide (PDI) and isoindigo [13–15]. The removal of the t-BOC is observed by the evolution of two gases CO_2 and isobutylene.

Amongst the various industrial pigment classes already exploited in organic electronics, Diketopyrrolopy-

***Corresponding Author: Luca Beverina:** Department of Materials Science, University of Milano, Via R. Cozzi, 55, Milano, Italy, I-20125
Myles Rooney, Riccardo Ruffo, Mauro Sassi: Department of Materials Science, University of Milano, Via R. Cozzi, 55, Milano, Italy, I-20125
Francesco Carulli, Silvia Luzzati: ISMAC-CNR, Via Corti 12, 20133 Milano, Italy
Roland Resel, Benedikt Schrode: Institute of Solid State Physics, Graz University of Technology, Austria

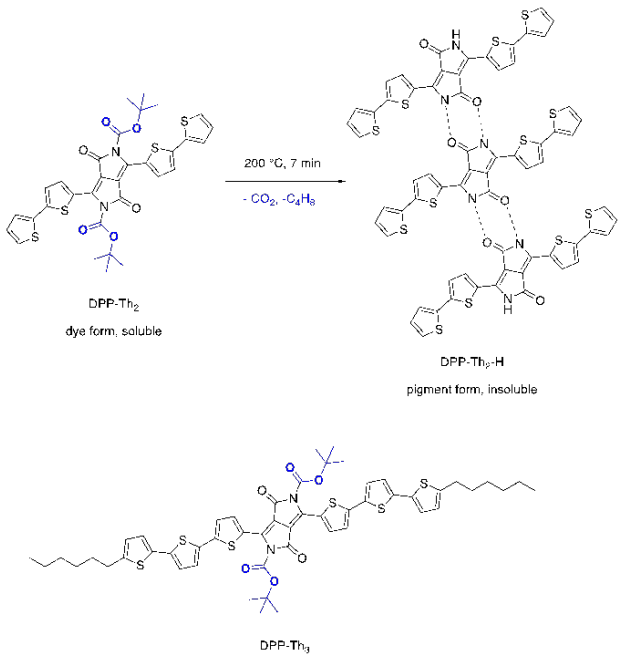

Fig. 1. Top: The latent pigment approach demonstrated on derivative DPP-Th_2. Bottom: The structure of latent pigment derivative DPP-Th_3

rroles (DPP) are recognised to be particularly successful. Probably the best known DPP pigment at an industrial level is Pigment 254, a.k.a. Ferrari red [16]. While this well known derivative has inappropriate HOMO/LUMO levels to be of practical value as an organic photovoltaic material, the chemistry of the DPP core has been extensively developed giving access to highly conjugated derivatives with good performances both in OPV and OFET technologies [17, 18]. It has been shown that in its parent pigment form DPP crystals have improved charge transport and mobilities over N-alkylated "dye" counterparts. This corresponds to the activation of a H-bonding network resulting in more efficient π-π packing [13]. These characteristics make DPP cores a perfect example for use with the latent pigment technique.

Recently, through our work to develop industrially compatible methods for creating cheap, green chemistry compliant organic semiconductors, we have demonstrated that the conjugation of simple DPP derivatives, bearing the protecting t-BOC functionality, can be extended via a modified Suzuki-Miyaura protocol in mild conditions in a water/micelle media. This procedure lead to the straightforward synthesis of derivatives DPP-Th_2 and DPP-Th_3 in high yield in an ambient atmosphere. (Figure 1) [19, 20].

Previously we have employed the simple di-tert-butyl3,6-di(biphenyl- 4-yl)-1,4-dioxopyrrolo[3,4-c]pyrrole-2,5(1H,4H)-dicarboxylate (DPP_{BOC}) small molecule derivative in the preparation of bulk heterojunction photovoltaic devices [5]. The thermal deprotection of DPP_{BOC} at 200°C was used to trigger a phase segregation effect with respect to PCBM, thereby accessing a favourable BHJ morphology by a post deposition technique. Photovoltaic characterisation demonstrated a remarkable increase in Jsc upon formation of cleaved 3,6-di(biphenyl- 4-yl)-1,4-dioxopyrrolo[3,4-c]pyrrole-2,5(1H,4H)-dicarboxylate (DPP_H) within the film. This resulted in a 20-fold increase power conversion efficiency with respect to the as prepared cells based on protected DPP_{BOC}. The increase in current was attributed both to the improved charge carrier mobilities, arising from the hydrogen bonding network which improves material packing and to improved charge generation due to the formation of an extended Donor-Acceptor interface. Conversion efficiencies peaked at a modest 0.15 % due to the relatively wide optical gap of DPP_H along with unfavourable level alignment with respect to PCBM. Here we report DPP materials with thiophene rings substituted in place of Phenyl rings in order to reduce the optical gap and raise the HOMO level of this molecule for increasing the spectral overlap to the sunlight spectrum and for a more suitable alignment with PCBM to favour charge separation at the hetero-interface.

2 Experimental

2.1 Materials and methods

All reagents were used as delivered from Sigma Aldrich and TCI chemicals without further purification. ITO patterned glass substrates were supplied by TFD Inc. with a work function of 4.8 eV. The thermal window for deprotection was measured by specular X-ray diffraction and thermogravimetric analysis.

For X-ray scattering experiments, thin films were prepared on silicon oxide wafers with 150 nm thermal silicon as surface coverage.

X-ray reflectivity measurements were carried out on an PANalytical Empyrean system using a sealed copper tube, the radiation was parallized and monochromatized with an X-ray mirror so that a primary x-ray beam was formed with a vertical height of 0.1 mm and CuKa radiation. Fitting of the reflectivity data was performed with the software X'Pert Reflectivity.

Grazing incidence X-ray diffraction (GIXD) measurements were performed at the Diamond Light Source (Didcot, UK), beamline I07 21. X-rays with a wavelength of 1.00 Å were used at an incident angle of ~0.12°, slightly below the critical angle of the substrate to reduce the back-

ground signal. Diffracted intensities were measured using a Pilatus 2M area detector. Reciprocal space maps were calculated from the measured data using the xrayutilities library for Python [22]. Extraction of peak positions and indexation was performed using the custom-made software PyGID [23].

Synthesis

DPP-Th_2 and DPP-Th_3 derivatives were prepared according to the literature procedure [19].

Preparation of the PMMA slabs

100 ml of freshly distilled methyl methacrylate is added to 100 mg of the free radical initiator azobisisobutyronitrile (AIBN). This mixture is stirred vigorously and heated slowly until just under the boiling point. The viscosity slowly changes. Heat until the solution becomes a viscous syrup. Evolving bubbles should be slow to rise through the solution. Quench this reaction in an ice bath to 20°C. In a separate beaker dissolve 150 mg of lauryl peroxide and the latent pigment of interest ($1x10^{-5}$M) in 60 ml of freshly distilled methyl methacrylate. This solution is added directly to the partially polymerised syrup. Stir until homogeneous before casting into a square mould. Heat the mould in a water bath for 24 hours at 58°C. Remove the slab from the mould and heat in an oven for a further 12 hours at 100°C to ensure complete polymerisation. The optical absorption of a series of PMMA slabs was measured using a Jasco v-570 Uv-spectrometer before and after thermal cleavage in a heated oil bath.

2.2 BHJ and bilayer device fabrication and characterisation

Bilayer devices were fabricated with the following protocol. ITO substrates underwent a standard sonication for 10 minutes subsequently in 2% mucasol solution, distilled water, acetone and isopropanol. Substrates were then dried under a nitrogen flow before 10 minutes ozone cleaning. PEDOT:PSS was then spincoated at 2000 rpm for 60 seconds before being annealed at 110°C for 10 minutes in a nitrogen glove box (45-50 nm). Active layer deposition was then carried out with DPP-Th_2 and DPP-Th_3 with 8.5 mg/mL solutions in chloroform spincoated at 4000 rpm for 45 seconds. The substrates were then placed on a hot plate for deprotection at 200°C for 7 minutes. The insolubility of the deprotected films allows PCBM to be also spincoated from a chloroform solution of 8 mg/ml at 5000 rpm for 45 seconds. LiF was evaporated as a 1 nm interlayer. Barium was thermally evaporated as an 8 nm interlayer. The cells were closed with 90-100 nm of thermally evaporated aluminium. Each substrate contains 4 cells and 3 substrates were used per fabrication with a total of 12 cells made in tandem per fabrication. The active area of each cell is 6.2 mm^2. BHJ cells were also created with DPP:PCBM (weight ratio 1:1) being spincast from chloroform simultaneously. Thermal deprotection was carried out on half of the cells while the other half were tested thermal treatment/annealing free. The current density-voltage measurements were performed directly in glovebox where the solar cells were assembled, with a Keithley 2602 source meter, under AM 1.5G solar simulation (ABET 2000).

3 Results and Discussion

Derivatives DPP-Th_2 and DPP-Th_3 were selected by taking into account the two weaknesses of the previously employed derivative DPP_H: HOMO energy levels lower than that of PCBM (leading to faulty level alignment) and an absorption spectrum covering only the high energy region of the UV-Vis spectrum (cut off at 560 nm). Indeed, both new materials feature the use of thiophene over benzene thus ensuring higher conjugation through improved planarity and increased π-electron density according to the π-excessive nature of thiophene. Derivative DPP-Th_3 in particular was already employed, in its pristine protected form, to prepare BHJ devices with moderate to good conversion efficiencies [24].

The HOMO levels of DPP-Th_2 and DPP-Th_3 were estimated from the corresponding Cyclic voltammetry plots reported in figure 2, which also shows the energy level diagram of both DPP derivatives, alongside with the previously employed DPP_H. The addition of Th_2 and Th_3 moieties to DPP backbone induces a reduction of pigments band gap and allows also a better energy level alignment with respect to PCBM. It should be noted that such energy levels refer to the protected, latent pigment form of the DPP derivatives. CV characterization of deprotected pigments is not possible due to their extremely low solubility in organic solvents. The effect of protecting a strong electron withdrawing group with the t-BOC functionality is the lowering of both the HOMO. As such, the thermally activated cleavage process should raise the HOMO levels, with beneficial impact on level offsets with respect to the PCBM acceptor.

The impact on optical properties is much more difficult to predict. Pigments are known to be affected by ag-

gregation both in solution and in the solid state. The most striking example of such an effect is quinacridone whose pigment form is deep purple while the corresponding latent pigment one is pale yellow [25].

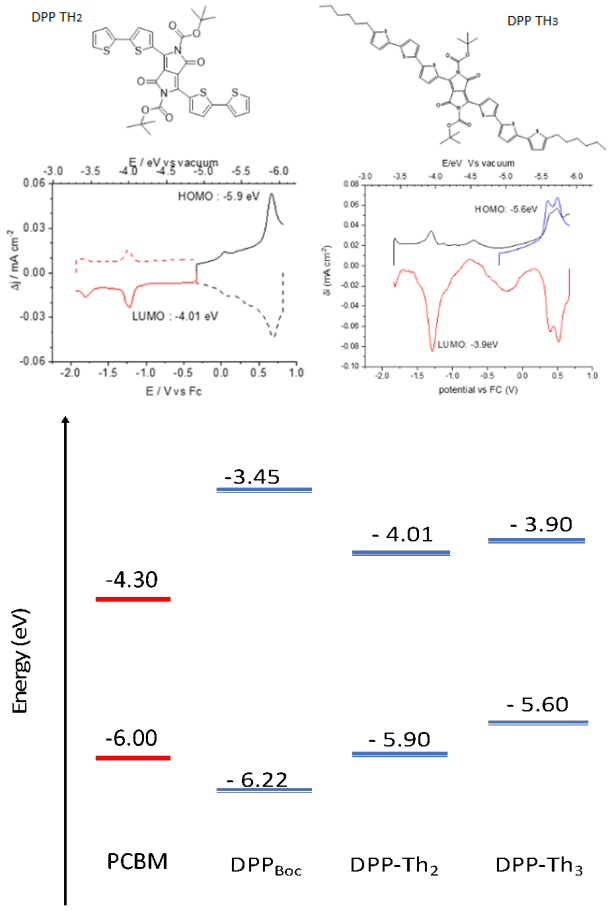

Fig. 2. Top: Cyclic voltammetry and structure of DPP-Th2 and Th3. Reversible redox steps evaluate HOMO levels to be –5.9 eV and 5.6 eV, LUMO levels of –4.01 eV and 3.9 eV respectively. Bottom: level diagrams for PCBM,[26] DPPH, DPP-Th$_2$, DPP-Th$_3$.

Indeed, unexpected absorption shifts and significant lowering of extinction coefficient after thermal cleavage of the t-BOC moiety was recorded. It is expected that the significant change in film crystallinity through deprotection of the latent pigment results in aggregation, leading to a shift in absorption wavelength, and an increase in light scattering throughout the film. However, this effect could also be intrinsic and due to the removal of the electron withdrawing t-BOC from the accepting residue of the DPP dyes. In order to be able to decouple the effects of aggregation from the single molecule effect of the cleavage, we resorted to the preparation of PMMA slabs incorporating DPP-Th$_2$ and DPP-Th$_3$ at very low concertation (to avoid aggregation), according to procedures elucidated from Luminescent Solar Concentrator fabrication processes [8].

Latent pigments are dissolved in a solution of PMMA in stabilizer free MMA. This viscous solution can be poured in a mould of suitable thickness (2 mm in our case). Polymerisation at a temperature well below the cleavage of the t-BOC unit affords a solid solution of latent pigment in PMMA. These slabs are then heated to 100°C to complete the polymerisation of all unreacted monomers and can undergo a further annealing in oil baths to deprotect the dispersed latent pigment within. The deprotection is performed on the unaggregated latent pigment within the high viscosity polymeric medium. Thus, we avoid the formation of aggregates as the pigments cannot appreciably diffuse. This strategy allows us to study the optical properties of the unprotected pigments behaving as highly dispersed molecules. Returning to the example of quinacridone, the deprotection of its latent pigment affords a yellow slab while the deprotection of its thin film equivalent gives very hazy purple layers.

PMMA slabs containing DPP-Th$_2$ and DPP-Th$_3$ were compared via UV-Vis spectroscopy before and after the cleavage with thin films measured using the same thermal cycle.

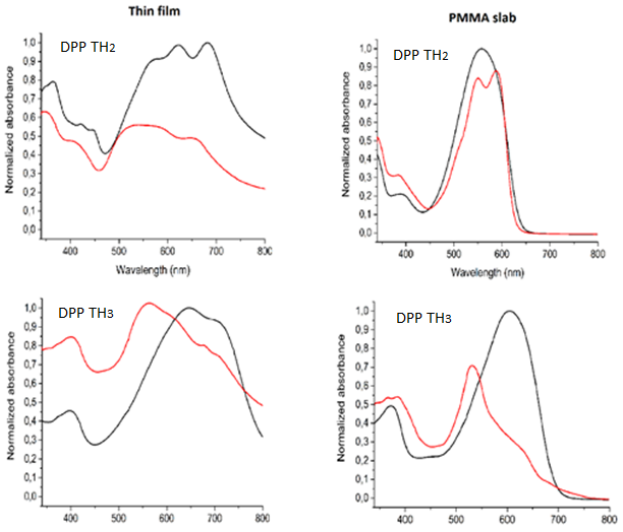

Fig. 3. Left) thin film UV absorption of DPP materials (Black) Protected (Red) After deprotection. Right) PMMA Slabs with DPP materials dispersed throughout. (Black) Protected (Red) After deprotection.

The behaviour of the two compounds is remarkably different. In the case of DPP-Th$_2$ the PMMA absorption spectra before and after the cleavage are similar both in terms of optical gap and oscillator strength. The main dif-

ference is the structuring of vibronic replicas going from the protected dye to the pigment form. This effect is coherent with the expected planarization due to the removal of the bulky t-BOC group. The comparison with the corresponding thin films clearly shows a remarkable tendency for aggregation, affecting both pristine and cleaved films. In both cases a band peaking at 700 nm attributed to a J type aggregate is clearly visible and survives the cleavage process. The optical density of the film is significantly reduced upon cleavage. The latter effect could be due to the formation of smaller crystallites, sizeably increasing the scattering of incident light. Such an interpretation is also supported by the GIXD data discussed later which shows quite clearly the formation of very small crystals.

As for DPP-Th_3 derivative, the behaviour is remarkably different. The PMMA slab shows the familiar low energy broad absorption band common to all DPP materials, in this case red-shifted due to the increased conjugation with respect to DPP-Th_2. Upon cleavage, a substantial widening of the optical gap is observed with shifting of the absorption maximum from 600 nm to 510 nm. Such a shift is connected with a sizeable reduction in the optical density. In this case, the planarization occurring as a consequence of the formation of intramolecular hydrogen bonds does not counterbalance the loss of electron withdrawing capability of the DPP core upon removal of the t-BOC residue. The thin film spectra show the same feature, along with a remarkable increase in the scattering background for cleaved samples, likely due to the same crystallization effect affecting derivative DPP-Th_2.

Such an effect can also be studied directly on thin films of DPP-Th_2 and DPP-Th_3 by X-ray reflectivity and GIXD before and after the thermal treatment. A strong change in the thin film morphology as well as in the crystalline properties is observed by X-ray reflectivity and GIXD, respectively. In detail, X-ray reflectivity investigations (see Supporting Information) were performed on spin coated films before and after the decoupling process. Fitting of the X-ray reflectivity curves reveal basic information on the thin film morphology. The films have a film thickness of 40 nm and 46 nm and show due to the decoupling process a reduction of the film thickness of 26% and 19% for the materials DPP-Th_2 and DPP-Th_3, respectively. The total electron densities of the film were determined by using the critical angle of total external reflection and converted to mass densities by the knowledge of the chemical composition. A value of 0.405 $Å^{-3}$ was obtained for DPP-Th2 which is smaller than 0.450 $Å^{-3}$ (mass density 1.430 g/cm^3), the calculated electron density for the molecule DPP-Th2 based on its single crystal solution. The decoupling process enhances the mass density of 4% and 10% for the materials DPP-Th_2 and DPP-Th_3, respectively. No change in the film roughness was observed for DPP-Th_2, a value of 2 nm was obtained by the X-ray reflectivity fit. For DPP-Th_3 the roughness increases from 1 nm to 3 nm due to the decoupling process.

GIXD patterns of spin coated films before and after the decoupling process are shown in Figure 4. The diffraction patterns of the as-prepared films (Figure 4a and 4b) are highly crystalline with strong preferred orientation of the crystallites. In case of the molecule DPP-Th_2 the diffraction peaks could be indexed. Based on the solved crystal structure (Figure 5) the positions of Bragg peaks are calculated and plotted together with the diffraction pattern (Figure 4a). A preferred orientation with the 001 planes parallel to the substrate surface is found. The agreement of calculated and experimentally observed peak positions is very good (e.g. compare for 0-10 and 011 / 0-11). Based on these results we can conclude that in case of DPP-Th_2, the single crystal structure is present within the spin coated films.

A drastic change in the diffraction pattern is observed after the decoupling process. The peaks are smeared more along Debye-Scherrer rings which means that the preferred orientation is less pronounced in comparison to the as-prepared films. The number of peaks is drastically reduced, and the peak width is considerably broader. This means that the crystalline order in the system is considerably decreased which is either related to a considerably smaller crystallite size or by increasing disorder within the individual crystalline domains. In case of DPP-Th_3 we observe Bragg peaks at q = 0.20 $Å^{-1}$ (d = 31 Å), q = 1.15 $Å^{-1}$ (d = 5.46 Å) and q = 1.83 $Å^{-1}$ (d = 3.43 Å) (Fig. 4d). In case of DPP-Th_2 we observe Bragg peaks at q = 0.33 $Å^{-1}$ (d = 19 Å) and q = 1.83 $Å^{-1}$ (d = 3.43 Å) (Fig. 4c).

The interplanar distance of 3.43 Å is dominantly present in both samples. This distance is the characteristic for π-π stacking distance of aromatic units. Interestingly, already the single crystal solution of DPP-Th_2 reveals stacks of the aromatic units with the comparable stacking distance of 3.47 Å. Comparing both diffraction peaks of the two different types of decoupled films there is a fundamental difference in the stacking of the aromatic units. In case of DPP-Th_2 the π-π stacks are oriented parallel to the substrate surface, since the diffraction peak is located around $q_{xy} = 0$. While in case of DPP-Th_3 the aromatic units are oriented perpendicular to the substrate surface, concluded from the presence of the diffraction peak located dominantly at $q_z = 0$.

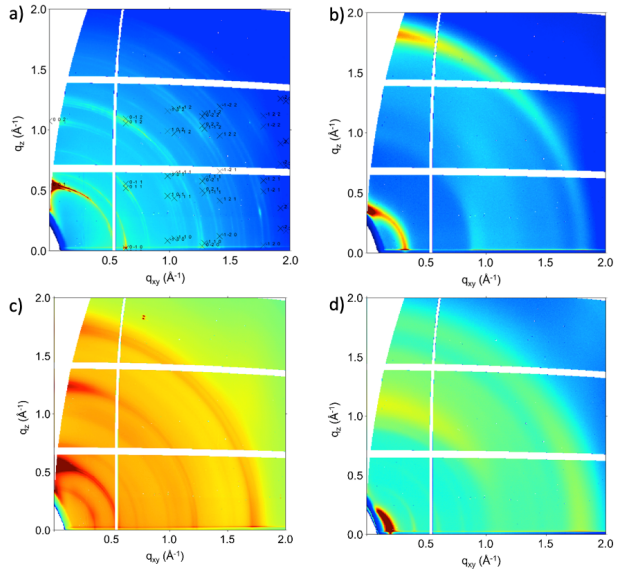

Fig. 4. a) Indexed GIXD of thin film of protected DPP-Th_2. b) GIXD of thin film of deprotected DPP-Th_2. c) GIXD of thin film of protected DPP-Th_3. d) GIXD of thin film of deprotected DPP-Th_3. Thick weak Bragg peaks seen as light blue bands indicate small crystallites with a random orientation in respect to the substrate. Diffraction plots have been converted into the scattering vector q space so that they are independent of wavelength of X-ray source.

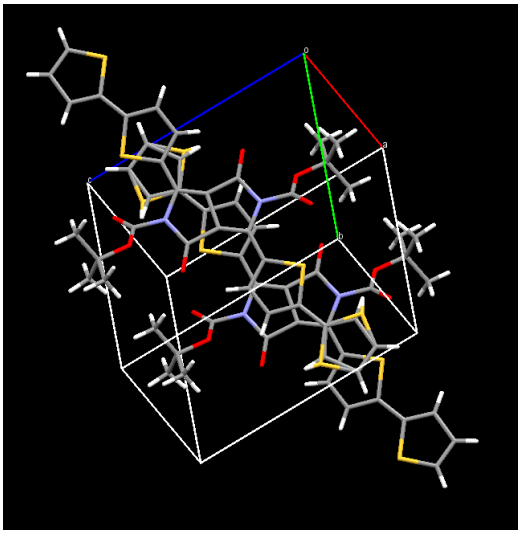

Fig. 5. Single crystal structure of DPP-$Th_2$was grown from slow evaporation in chloroform.

3.1 Bilayer Heterojuction devices

Bilayer heterojuction devices based on derivatives DPP-Th_2 and DPP-Th_3 were prepared and thermally annealed according to the protocol described in the materials and method section.

Preliminary device results for DPP-Th_2 show a moderate PCE of 0.31%. Although this result is not outstanding when compared with benchmark figures for organic devices it does represent an almost doubling of the PCE% of previous Latent Pigment materials. This improvement is attributed to frontier orbital alignment between donor and acceptor within this cell.

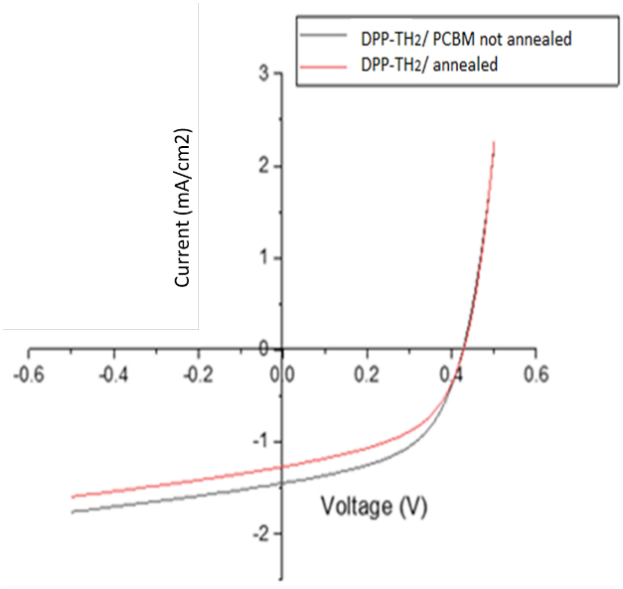

Fig. 6. Initial JV curve for *ITO/PEDOT:PSS/ DPP-Th_2/PCBM/LiF/Al* bilayer device.

A short post deposition annealing of 140°C for 5 minutes was carried out on closed *ITO/PEDOT:PSS/DPP-Th_2/PCBM/LiF/Al* cells. Results are shown in Table 1.

This is a standard post deposition annealing procedure which improves the interface mixing of the layers and should not be confused with the thermal cleavage of the latent pigment, happening at 200°C prior to the deposition of the acceptor layer and contacts closing the cell. This secondary annealing resulted in a noticeable reduction in short circuit current. LiF provides an ohmic contact between semiconductor and metal contact and lowers the work function of aluminium. Lithium has also been observed migrating into active semiconductor layers, usually this lithium doping of the organic results in improved device performances [27]. Improvements to FF and Voc due to an optimised charge transfer across the interface is also commonly seen with the use of this interlayer [28–30]. However, LiF can also crystalize into heterogeneous plate islands on the surface of semiconductors resulting in non-optimum interlayer properties.

To investigate the possible effects of LiF dissipation during annealing, a similar close cell thermal treatment was also carried out using Ba rather than LiF.

Table 1. Results of the annealing process carried out on a *ITO/PEDOT:PSS/ DPP-Th$_2$/PCBM/LiF/Al* bilayer device at 140°C for 5 minutes on closed cell, i.e. after the LiF/Al electrode evaporation. The remeasured cell showed a reduction in current and fill factor.

Sample	Voc [V]	FF [%]	Jsc [mA/cm^2]	PCE [%]
Not annealed (closed cell)	0.43	0.50667	1.44	0.31%
140°C annealed (closed cell)	0.45	0.38032	1.33	0.23%

Table 2. *ITO/ PEDOT:PSS/ DPP-Th2/ PCBM/ interlayer/Al* bilayer device results. Average device data taken over 12 cells for each interlayer and annealing treatment.

	Voc [V]	Jsc [mA/cm^2]	FF [%]	PCE %]
Barium	0.455	0.96491	0.431655	0.19
Barium annealed	0.441	1.254683	0.46415	0.2571
LiF	0.3975	1.4558	0.4987875	0.2882
LiF annealed	0.436	1.295613	0.3739425	0.2117

Interestingly the closed cell annealing in the case of devices fabricated with barium improves the device performance contrasting with the behaviour of LiF. This may suggest that LiF is indeed forming non-uniform islands upon annealing.

The further symmetrical extension of the DPP-Th$_2$ core with a further hexyl thiophene to form the DPP-Th$_3$ structure was thought as a facile means to enhance the Jsc. Unfortunately, the desired Voc was not achieved when DPP-Th$_3$ was fabricated into bilayer devices. The average short circuit current for devices fabricated with DPP-Th$_3$ increases but the Voc decreases in comparison to DPP-Th$_2$, this is consistent with the electronic modifications of the materials. Film thicknesses was optimised by adapting the spincoating speed for the deposition of the donor layer. By increasing the thickness of this active layer, we see a very small improvement in the fill factor of the devices (see table 3 below). Unlike DPP-Th$_2$ further thermal annealing after deposition of PCBM at 140°C for 5 minutes does not appear to have a substantial effect on device performance.

4 Conclusion

A latent pigment strategy has been developed to fabricate planar bilayer organic photovoltaics. Two lead diketopyrrolopyrrole (DPP-Th$_2$ and DPP-Th$_3$) based semiconductors were chosen for a detailed study in both device characteristics and film quality. The small molecules in question undergo a significant crystallographic rearrangement upon the thermal cleavage of solubilising groups. A significant reduction in crystal size is noted with a resulting powder-like film. No crystal orientation is observed after deprotection. The result is a disordered and more than likely permeable layer of material. The device characterisation shows evidence of poor charge generation and a high level of thermal instability in terms of bulk morphology. This is most likely attributed to permeability of the donor layers due to the formation of very small crystals upon thermal cleavage of the latent pigment form. Upon heating permeable channels are available for PCBM to migrate through causing unbalanced, weakly performing devices which have a structure more similar to an intermixed bilayer or bulk heterojunction device. The highest performing devices for these materials was 0.33% PCE averaged over 12 devices. This is double the power conversion efficiency previously produced by a bulk heterojunction of DPP$_H$/PCBM. The improvements in performance is accounted to alignment of HOMO and LUMO levels between donor and acceptor. PMMA slabs containing highly dispersed latent pigments were created in order to examine the optical properties of the latent pigments and the effects of agglomeration and crystalline properties on the absorptive properties of these materials in thin films. A shift in the absorption spectra is accounted for by the electron withdrawing nature of t-BOC on each of the materials examined. It is established that the decrease in extinction coefficient seen during deprotection is greatly exaggerated for a thin film on a substrate compared to the highly dispersed materials trapped within the bulk PMMA. It is evident that less crystalline order and agglomerative tendencies of the deprotected films has an adverse effect on the absorption properties of these materials. High level of crystalline order with low levels of material interconnectivity seems to work against the device performances.

Acknowledgment: We thank Università degli Studi Milano-Bicocca (grant n° 2016-ATESP-0047) and MIUR (Progetto Dipartimenti di Eccellenza 2017 “Materials for energy”) for financial support. L.B. and M.R. thank the

Table 3. Device characteristics for ITO/PEDOT:PSS/ DPP-Th_3/PCBM/LiF/Al cells. All data is averaged over 3 substrates containing 4 cells each.

DPP-Th_3 spin speed and post-deposition annealing 140°C	Voc [V]	Jsc [mA/cm^2]	FF%	PCE%
8 mg/ml 2000 rpm thermally annealed	0.369	2.186	39.21	0.317
8 mg/ml 1000 rpm thermally annealed	0.371	2.099	42.33	0.329
8 mg/ml 800 rpm thermally annealed	0.375	2.105	42.58	0.336
8 mg/ml 1000 rpm as cast	0.368	2.277	39.40	0.330
8 mg/ml 800 rpm as cast	0.353	2.242	42.23	0.334

European Community's Seventh Framework Programme (FP7/2007-2013) under grant agreement N. 607232 for financial support (THINFACE).

The authors also thank Diamond Light Source for access to beamline I07 (proposal SI13569-1).

References

[1] Rochester, C. W., Mauger, S. A. & Moule, A. J. Investigating the Morphology of Polymer/Fullerene Layers Coated Using Orthogonal Solvents. *J. Phys. Chem. C* **116,** 7287–7292 (2012).

[2] Gevaerts, V. S., Koster, L. J. A., Wienk, M. M. & Janssen, R. A J. Discriminating between bilayer and bulk heterojunction polymer:fullerene solar cells using the external quantum efficiency. *ACS Appl. Mater. Interfaces* **3,** 3252–5 (2011).

[3] www.heliatek.com

[4] J. S. Zambounis, Z. Hao, A. I. Latent pigments activated by heat. *Nature* **388,** 131–132 (1997).

[5] Bruni, F. *et al.* Post-deposition Activation of Latent Hydrogen-Bonding: A New Paradigm for Enhancing the Performances of Bulk Heterojunction Solar Cells. *Adv. Funct. Mater.* 1–10 (2014). doi:10.1002/adfm.201400896

[6] Chen, T. L., Chen, J. J. A., Catane, L. & Ma, B. Fully solution processed p-i-n organic solar cells with an industrial pigment - Quinacridone. *Org. Electron. physics, Mater. Appl.* **12,** 1126–1131 (2011).

[7] Galliani, D. *et al.* Thermochromic Latent-Pigment-Based Time – Temperature Indicators for Perishable Goods. 1164–1168 (2015). doi:10.1002/adom.201500073

[8] Mattiello, S., Sanzone, A., Brazzo, P., Sassi, M. & Beverina, L. First Demonstration of the Applicability of the Latent Pigment Approach to Plastic Luminescent Solar Concentrators. 5723–5729 (2015). doi:10.1002/ejoc.201500554

[9] Maqueira-Albo, I. *et al.* A latent pigment strategy for robust active layers in solution-processed, complementary organic field-effect transistors. *J. Mater. Chem. C* **5,** 11522–11531 (2017).

[10] Liu, T. H., Cheng, W. T. & Huang, K. T. Crystallization and morphology of indanthrone converted from latent pigment in the solution with photo acid generator. *Dye. Pigment.* **105,** 137–144 (2014).

[11] Głowacki, E. D. *et al.* A facile protection–deprotection route for obtaining indigo pigments as thin films and their applications in organic bulk heterojunctions. *Chem. Commun.* **49,** 6063–6065 (2013).

[12] Wuts, P. G. M. *Protective Groups in Organic Synthesis*. (1999).

[13] Głowacki, E. D. *et al.* Hydrogen-bonded diketopyrrolopyrrole (DPP) pigments as organic semiconductors. *Org. Electron.* **15,** 3521–3528 (2014).

[14] Jones, F. & Okui, N. The Thermal Stability of Linear Trans-quinacridone Pigments. *Soc. Dye. Colour.* **91,** 361–365 (1975).

[15] Moreno-lo, J. C., Grizzi, O. & Sa, E. A. Thermal Stability of N,N′-Bis(1-ethylpropyl)perylene-3,4,9,10-tetracarboxdiimide Films on Cu(100). *J. Phys. Chem. C* **120,** 19630–19635bro (2016).

[16] Chandran, D. & Lee, K. Diketopyrrolopyrrole: A Versatile Building Block for Organic Photovoltaic Materials. **21,** 272–283 (2013).

[17] Arias, A. C., Mackenzie, J. D., Mcculloch, I., Rivnay, J. & Salleo, A. Materials and Applications for Large Area Electronics: Solution-Based Approaches. *Chem. Rev.* **110,** 3–24 (2010).

[18] Vezie, M. S. *et al.* Exploring the origin of high optical absorption in conjugated polymers. *Nat. Mater.* **15,** (2016).

[19] Rooney, M. *et al.* Suzuki-Miyaura cross-coupling of latent pigments in water/toluene emulsion under aerobic atmosphere. *Dye. Pigment.* **149,** 893–901 (2018).

[20] Mattiello, S. *et al.* Suzuki-Miyaura Micellar Cross-Coupling in Water, at Room Temperature, and under Aerobic Atmosphere. *Org. Lett.* **19,** 654–657 (2017).

[21] Nicklin, C., Arnold, T., Rawle, J. & Warne, A. Diamond beamline I07: a beamline for surface and interface diffraction. *J. Synchrotron Radiat.* **23,** 1245–1253 (2016).

[22] Kriegner, D., Wintersberger, E. & Stangl, J. xrayutilities: a versatile tool for reciprocal space conversion of scattering data recorded with linear and area detectors. *Appl. Crystallogr.* **46,** 1162–1170 (2013).

[23] Moser, A. Thesis. (Graz University of Technology, Austria, 2012., 2012).

[24] Tamayo, A. B., Walker, B. & Nguyen, T.-Q. A Low Band Gap, Solution Processable Oligothiophene with a Diketopyrrolopyrrole Core for Use in Organic Solar Cells. *J. Phys. Chem. C* **112,** 11545–11551 (2008).

[25] Głowacki, E. D. *et al.* Hydrogen-Bonded Semiconducting Pigments for Air-Stable Field-Effect Transistors. *Adv. Funct. Mater.* **25,** 1563–1569 (2013).

[26] Scharber, B. M. C. *et al.* Design Rules for Donors in Bulk-Heterojunction Solar Cells — Towards 10 % Energy-Conversion Efficiency. *Adv. Mater.* **5090,** 789–794 (2006).

[27] Bruder, F. & Brenn, R. Photoelectron Spectroscopy of the Contact between the Cathode and the Active Layers in Plastic Solar Cells: The Role of LiF. *Jpn. J. Appl. Phys.* **44,** 3695 (2005).

[28] Brabec, C. J. *et al.* Effect of LiF / metal electrodes on the performance of plastic solar cells. *Appl. Phys. Lett.* **80,** 1288 (2002).

[29] Lee, S., Jeong, S., Kim, D., Kim, C. & Han, Y. Inverted Polymer Solar Cells with an Ultrathin Lithium Fluoride Buffer Layer. *J. Nanosci. Nanotechnol.* **12,** 3205–3209 (2012).
[30] Ahlswede, E. *et al.* Comparative study of the influence of LiF , NaF , and KF on the performance of polymer bulk heterojunction solar cells bulk. *Appl. Phys. Lett.* **90,** (2007).